IEEE Access
Multidisciplinary | Rapid Review | Open Access Journal

Received March 31, 2020, accepted April 20, 2020, date of publication April 24, 2020, date of current version May 8, 2020.

Digital Object Identifier 10.1109/ACCESS.2020.2990357

Dynamic Compensation of Path Length Difference in Optical Coherence Tomography by an Automatic Temperature Control System of Optical Fiber

DAEWOON SEONG[1], SANGYEOB HAN[1], DEOKMIN JEON[1], YOONSEOK KIM[1], RUCHIRE ERANGA WIJESINGHE[2,3], NARESH KUMAR RAVICHANDRAN[1,6], JAEYUL LEE[1], JUNSOO LEE[1], PILUN KIM[4], DONG-EUN LEE[5], MANSIK JEON[1], (Member, IEEE), AND JEEHYUN KIM[1], (Member, IEEE)

[1]School of Electronics Engineering, College of IT Engineering, Kyungpook National University, Daegu 41566, South Korea
[2]Department of Biomedical Engineering, College of Engineering, Kyungil University, Gyeongsan 38428, South Korea
[3]Department of Autonomous Robot Engineering, College of Smart Engineering, Kyungil University, Gyeongsan 38428, South Korea
[4]School of Medicine, Institute of Biomedical Engineering, Kyungpook National University, Daegu 41944, South Korea
[5]School of Architecture and Civil Engineering, Kyungpook National University, Daegu 41566, South Korea
[6]Center for Scientific Instrumentation, Korea Basic Science Institute, Daejeon 34133, South Korea

Corresponding authors: Dong-Eun Lee (dolee@knu.ee.kr) and Mansik Jeon (msjeon@knu.ac.kr)

This work was supported by the National Research Foundation of Korea (NRF) Grant funded by the Korean Government, Ministry of Science and ICT (MSIT), under Grant 2018R1A5A1025137.

ABSTRACT Optical fiber is widely used in optical coherence tomography (OCT) to propagate light precisely with low attenuation and low dispersion. However, the total optical path length within the optical fiber varies in accordance with changes of the temperature. This leads changes in the total optical travel path of the interfering signals and results in shifting of OCT image position to an unintended depth pixel value. In this paper, we presented the temperature-based automatic path length compensating method in OCT to limit the external temperature effect and control the image position in micro-scale without manual movement of optical components. By utilizing developed hardware and software of automatic temperature control system, the external temperature of optical fiber is precisely regulated that evokes thermal expansion and finally changes the physical length of fiber, which is main mechanism of temperature-based path length compensating method. The effectiveness of the presented method was verified by two-dimensional OCT images of mirror and *in vivo* retina. The obtained results confirmed the path length variance due to temperature change is computable and can be regulated in real-time for whole pixel range of OCT image. Therefore, the proposed temperature-based path length compensating method can be used as an alternative method to precisely control the position of OCT image, while eliminating the effect of external temperature and apply to effectively configuring compact optical systems.

INDEX TERMS Optical fiber, automatic temperature control system, thermal expansion, micro position control, optical coherence tomography.

I. INTRODUCTION

Optical coherence tomography (OCT) is a non-destructive and high-resolution interferometric optical imaging technique that provides depth-resolved images in real-time [1], [2]. OCT has been employed in diverse applications, where cross-sectional imaging is requisite; few such areas include ophthalmology [3]–[5], dermatology [6], [7], dentistry [8], [9], gastroenterology [10], [11], cardiology [12], [13] and in pulmonology studies [14], [15]. Optical fiber-based OCT systems are widely used, as they can be helpful in transferring light easily and precisely with low attenuation and low dispersion [16]–[19]. Optical fiber confines and propagates the light along with its core, which is

The associate editor coordinating the review of this manuscript and approving it for publication was Md. Selim Habib.

fabricated from high refractive index materials. Various kinds of fibers, such as single-mode [20], multimode [21], [22] or polarization-maintaining fiber [23] are widely used as per need. However, materials of both core and cladding are subject to thermal expansion [24], [25] due to environmental factors, and this results in changes in the physical properties of the optical fiber.

When it comes to fiber optics-based OCT systems, the path lengths of the reference and sample arm should be matched within the coherence length of the light source to obtain an interference signal [2]. Subsequently, this means the slightest change of coherence length may affect the interfering signals, which in turn affects the obtained result of OCT image. Among the various factors of affecting the path length variance, the variance of external temperature is a well-understood concept [26]. To minimize the changes in travel path of the propagating light from varying temperatures, the cladding of fiber is usually silicone coated and wrapped in a protective outer jacket. As an alternative approach to compensate for changes in total travel path of light resulting from varying temperatures, a heat-insensitive interferometer was fabricated using a fiber loop mirror as reported in [27]. Similarly, a thermal silicon ring resonator fabricated by overlaying a polymer around silicon waveguides was reported as an option to overcome the aforementioned problem [28].

As mentioned in above paragraph, compensating path length difference should be controlled since the signal to noise ratio (SNR) of the system decreases as the imaging depth range increases [29], [30]. To compensate the path length difference, manual or motor-driven implementations are conventionally used. Manual adjustment can be subject to user error, and it is constrained to the degree of attainable fine-tuning. Subsequently, this led to the rising need for motorized movement. Motorized control movement of the optical components can enable the user to adjust the distance between the optical components in the micrometer scale [31], [32]. The piezoelectric motor is opted-in surgical and endoscopic OCT applications, where precise control of optical components is needed, this is to minimize the effect of micro-motion during measurements [33], [34] and it is more convenient when compared to manual adjustment. However, the operating range of the piezoelectric motor is not wide, compared with translational stage, and the operating range of motorized stage is limited due to its spatial constraint. To overcome the aforementioned limitations, optical delay line has been made and implemented in OCT to maintain the path length. However, due to the necessity of additional optical components to compose the optical delay line, the unexpected dispersion and loss can occur [35], [36].

In this study, we propose a novel path length compensating method for maintaining the OCT image position by directly varying the overall temperature of a selective region in the optical fiber, which is able to control the wide depth range of OCT image in real-time. To precisely regulate the temperature of each interference arms, the automatic temperature control system was developed and controlled with customized software using LabVIEW. To reach and maintain a set temperature, pulse width modulation (PWM) and proportional integral derivative (PID) feedback control were used to design the control software. The proposed system is adept at varying the optical fiber temperature within the range of 10 °C to 60 °C. The system performance was evaluated by imaging mirror sample at various temperature conditions. In addition, to evaluate the effect of temperature and its length dependency of optical fiber in OCT imaging, we obtained two-dimensional (2D)-OCT images using 2 m and 5 m long optical fibers at different temperatures. Additionally, by utilizing the proposed system, we obtained *in vivo* retina image to evaluate the attainable path length compensating range using the proposed system.

II. MATERIALS AND METHODS

A. OCT SYSTEM SETUP

Fig. 1(a) is a schematic of the SD-OCT hardware setup. A super-luminescent diode (EXS210068-01, Exalos, Swiss), is used for the broadband light source; it has an 854 nm center wavelength and a 53 nm full width at half maximum bandwidth. The light from the laser source was transmitted to a fiber coupler (50:50, TW850R5A2, Thorlabs, USA) to attain the Michelson interferometer configuration. The beam is then divided into a reference arm and a sample arm path. To investigate the overall effect of temperature control, we used 2 m patch cables (P3-830A-FC-2, Thorlabs, USA) connected using an FC/APC mating sleeves (ADAFC3, Thorlabs, USA) to deliver light. Additionally, we also used 5 m patch cables to investigate the effective changes by the temperature control system when using an extended fiber cable. It is worthy to note that the automatic temperature control system is directly connected to the reference arm and the sample arm of the optical fiber in all experiments. Signals delivered to the control system are managed by a data acquisition (DAQ) module (PCIe 6321, National Instruments, USA) hosted in a personal computer that executes the LabVIEW software-based controller algorithm. The reference arm comprises a collimator (F260APC-780, Thorlabs, USA), achromatic doublet (AC254-050-B) lens for focusing the incident collimated beam on to a protected silver mirror (PF10-03-P01, Thorlabs, USA). A collimator of exactly similar specification is used to deliver the laser beam to the sample arm and 2D and three-dimensional (3D) scanning are achieved by using a galvanometer scanning system (GVS012, Thorlabs, USA). Followed by the galvanometer scanning mirrors, an achromatic doublet (AC254-050-B) lens is used to focus the incident laser beam on the sample surface. The backscattered light from the reference and sample arms generated an interference fringe signal in the fiber coupler. The signal is detected by a customized spectrometer, which is detailed described in [37].

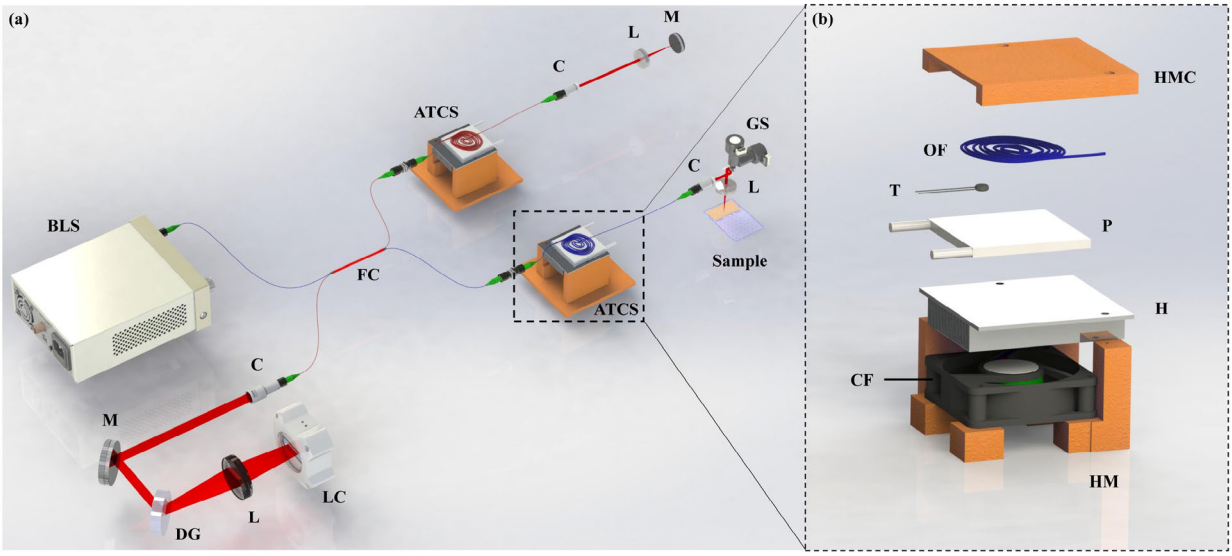

FIGURE 1. Schematic of the OCT system and photograph of laboratory customized automatic temperature control system. (a) shows an overall system schematic of OCT system used in this experiment. (b) shows specific hardware composition of automatic temperature control system. ATCS, automatic temperature control system; BLS, broadband laser source; C, collimator; CF, cooling fan; DG, diffraction grating; FC, fiber coupler; GS, galvanometer scanner; H, heatsink; HM, holding mount; HMC, holding mount cover; L, lens; LC, line scanning camera; M, mirror; OF, optical fiber; P, Peltier device.

B. HARDWARE CONFIGURATION OF THE AUTOMATIC TEMPERATURE CONTROL SYSTEM

Two automatic temperature control systems consist of Peltier device, thermistor, solid-state relay, heat sink, and cooling fan, are attached respectively to the reference arm and the sample arm of the optical fiber. The schematic diagram of hardware composition is demonstrated in Fig. 1(b), which is consisted of aforementioned electronic devices with customized 3D-printer based holding mount. The Peltier device plays a key role in regulating the temperature, while it provides both heating and cooling depending on the current passing direction. The current direction is determined by the difference between the detected current temperature and the predetermined temperature that is to be maintained, which is controlled by an output from the DAQ. The solid-state relay works as an electrical switch to reliably control the Peltier device. Additionally, the heatsink and cooling fan are used to cool the Peltier device. The total length of the optical fiber in contact with the Peltier device is 1.4 m of the optical fiber at each arm. The thermistor is placed to be in contact with the Peltier device surface to continuously monitor the temperature around the patch cable. The temperature of the two optical fibers (reference and sample arm) in the OCT system are controlled by an automatic temperature control system. Apart from the sample and reference arms (output ports) of the fiber, the rest of the fiber is void of any changes in hardware setup, as the generated interference signal is not directly affected by the automatic temperature control system. In addition, to precisely place and integrate the electronic components, we designed and produced the holding mount shown in Fig. 1(b) using 3D-printer. By using a customized holder of automatic temperature control system, the temperature of both fibers is controlled under the equivalent condition.

C. SOFTWARE ALGORITHM FOR THE AUTOMATIC TEMPERATURE CONTROL SYSTEM

The two main concepts incorporated in the software algorithm are PWM and PID feedback control. PWM is widely used to control the LED brightness and the motor speed by changing the duty cycle of a square wave power source. In our temperature control system, the duty cycle was controlled by the PWM to reach the desired value. Manual adjustment of a duty cycle is usually inaccurate and difficult to execute for an immediate response. Hence, a PID feedback control is used in the algorithm. PID is a feedback control method, which changes the system input in real-time according to the difference between the output and reference input to reach the set value. For effective utilization of the PID feedback control, the coefficients Kc, Ti and Td, which determines the accuracy and speed of the control, are set to with a predefined value as per best suit.

The software algorithm for adjusting the temperature to the desired value is shown in Fig. 2. For easier interpretation, the operations are divided into PC, DAQ, and automatic temperature control systems, with green, brown, and blue color borders, respectively. The system was initialized by setting the desired temperature and selecting the appropriate coefficients for feedback. The resistance value of the thermistor is continuously measured, which offers the current temperature of the fiber cables. The difference between the desired set temperature and measured current temperature determines whether the Peltier device should execute the heating or cooling operation. In order to reach the set temperature as

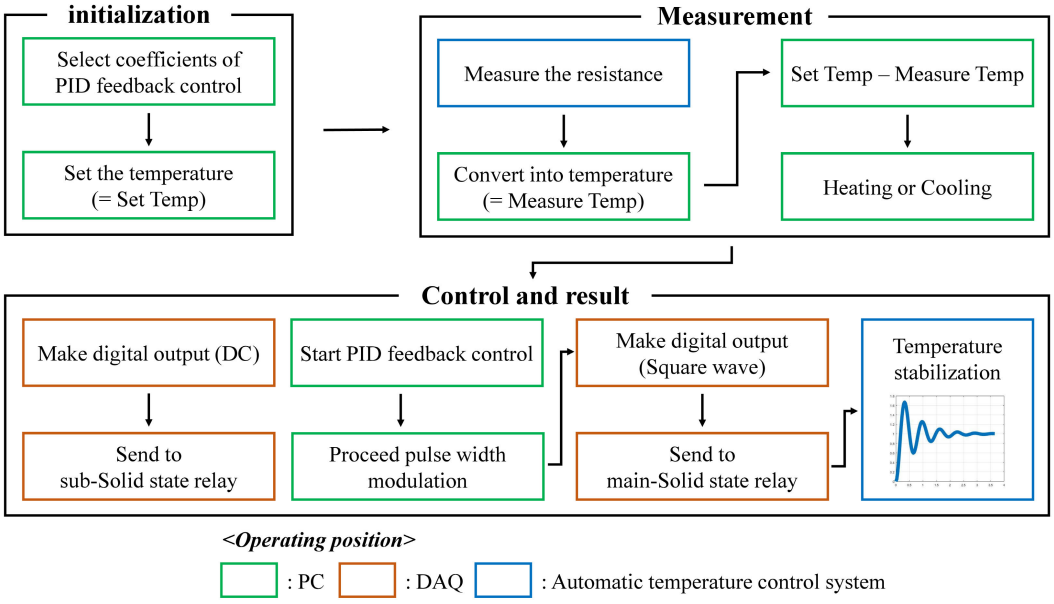

FIGURE 2. Software algorithm of the proposed system to reach and maintain the desired temperature. The border color of each box signifies the operating position. PC, personal computer. PID, proportional integral derivative.

quickly as possible, the feedback control is proceeded based on the temperature difference. The PWM conducted at a rate of 50 Hz by the PID feedback control and the calculated duty cycle is transferred to the main-solid state relay, which controls the operation time per cycle of Peltier device. With this continuous temperature control process, the temperature was reached to the predefined desired value, and it is maintained by the continuous operation as explained.

To better explain the temperature control cases, the descriptions of hardware movement compared with linear stage based method are shown in Fig. 3. At conventional method shown in the first row of Fig. 3, the path length was changed according to the direction indicated by the blue arrow as the reference of zero-path delay. Similarly, at the temperature control-based method, the temperature of fibers (both reference and sample arm) are regulated to generate the equivalent path length compensation effect of conventional method. Therefore, throughout the article, each case of proposed method can be corresponded to 4 cases of conventional method shown in Fig. 3.

III. RESULTS

A. 2D-OCT IMAGES AT REPRESENTATIVE TEMPERATURES WITH DIFFERENT LENGTH OF FIBER

To test the capability of path length control in longer ranges up to millimeters, the temperatures of the reference and sample arms were set to a wider range between 10 °C and 60 °C with multiple temperature selections within this range, which is proper bounds that optical fiber can conduct the equivalent performance. Throughout the article, the temperatures of the reference arm and sample arm used in the experiments are presented as ‘‘(the value of reference arm temperature (°C), the value of sample arm temperature (°C))’’ in the text. The cross-sectional OCT images obtained in this range using 2 m fiber are shown in Fig. 4(a)-(i). We selected the temperatures (10, 60) to observe the change in OCT image position when the interfering arms are at the highest optical path delay, which can be observed within the maximum range of line-scan camera. As the temperature of reference arm increased and the temperature of sample arm decreased, the rising tendency of the OCT image position can be seen in Fig. 4(a)-(i). Fig. 4(m) is the combined graph of each A-scan profile of all the measured results using 2 m fiber from (10, 60) to (60, 10). Fig. 4(m) shows that the pixel position of the intensity peak in the A-scan graph is increased (towards the pixel number 800), and the OCT image position is moved downward as the temperature changes. The pixel number of the detected intensity peak and from the respective displacement of the OCT images are given in Table 1. The OCT image obtained at (10, 60) and its respective measured value is taken to be the reference point to calculate the displacement of the OCT image as the temperature is changed. The maximum observed displacement of the OCT image was 461 pixels, which converts to 2005.35 μm.

To observe the impact of optical fiber length when a temperature-based path control system is used for OCT image position maintenance, a 2 m and 5 m length patch cable is connected to the subsequent experimented sample and reference arms. A 2.8 m length of the 5 m patch cable is subject to the automatic temperature control system, and this is twice the length used for the 2 m optic fiber cable (which was 1.4 m). Fig. 4(j)-(l) are the obtained representative 2D-OCT images of a mirror sample, using 5 m fiber at representative

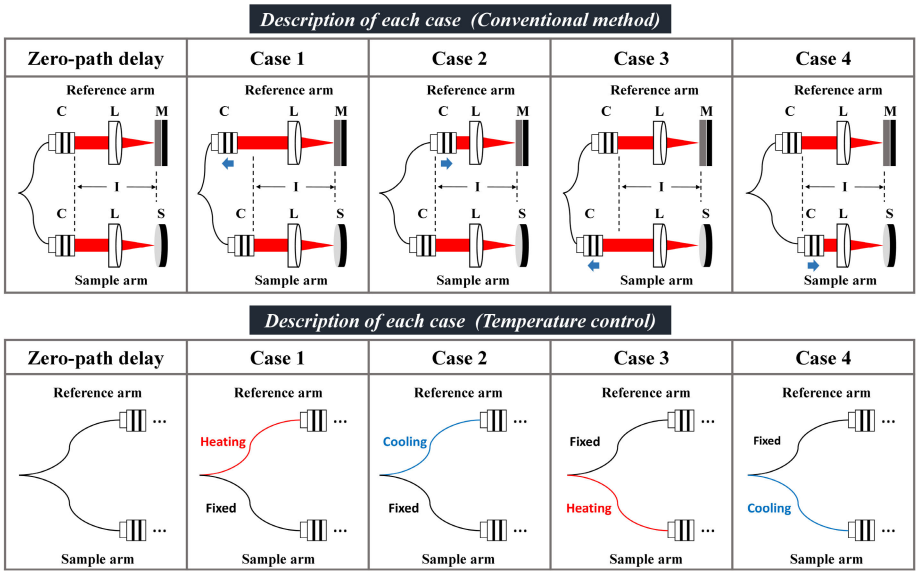

FIGURE 3. Description of each path length compensation cases utilized automatic temperature control system-based method compared with conventional method using linear stage.

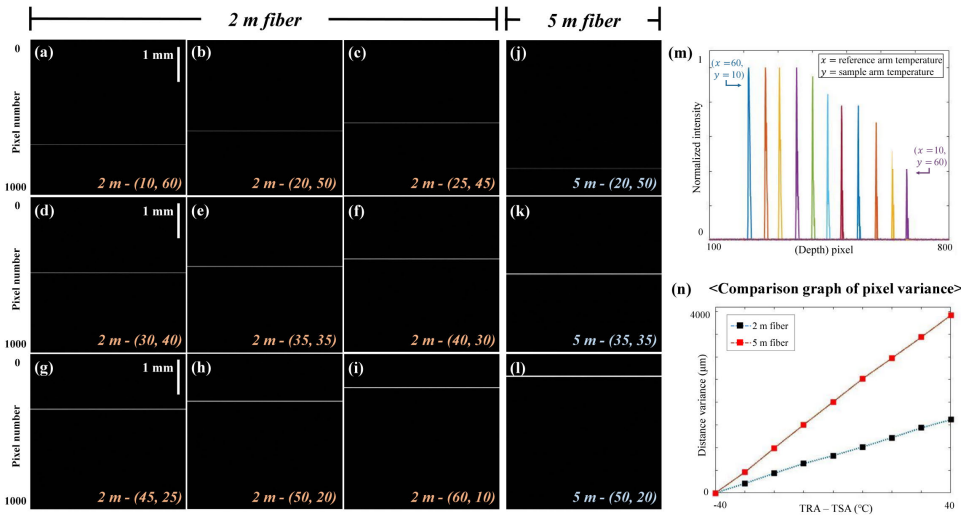

FIGURE 4. Obtained 2D-OCT images at various temperatures using two different length of fiber and the respective plotted graphs. The temperatures of the reference arm and sample arm used in this figure are presented as "(the value of reference arm temperature (°C), the value of sample arm temperature (°C))". (a)-(i) are 2D-OCT images of a mirror at different selective temperatures using 2 m fiber. (j)-(l) are the representative 2D-OCT images using 5 m fiber. (m) is a combined A-scan graph obtained from OCT images using 2 m fiber recorded at temperatures from (60, 10) to (10, 60). From (60, 10), temperature of reference arm decreased is by 5 °C while the temperature of the sample arm is increased by 5 °C. (n) shows the linear correlation between the temperature change and distance variance in the OCT images using 2 m and 5 m fiber. TRA, temperature of reference arm; TSA, temperature of sample arm.

temperatures of (20, 50), (35, 35), and (50, 20). Under the identical temperature conditions of 2 m fiber, the displaced OCT image positions as a function of the difference in optic fiber length are shown in Fig. 4(j)-(l). To demonstrate the validity of this result quantitatively over a wider range of temperatures, the position variation in the OCT images for a 5 m optic fiber is indicated with red squares in Fig. 4(n) compared with the results presented in Table. 1, which is the result of using 2 m optical fiber represented as black squares. The x-axis of the graph is the temperature difference between the reference arm and sample arm, and the y-axis is the distance between the observed pixel number of the intensity peak. Fig. 4(n) shows the linear increasing tendency between the temperature difference and the displaced OCT images when connected with the 2 m and 5 m fibers. In addition, the measured displacement of the OCT image for 5 m is

TABLE 1. Calculated data of pixel difference and distance change according to the varying temperature.

Reference Temperature (°C)	Sample Temperature (°C)	Pixel (depth) position	Pixel difference	Image Displacement (μm)
10	60	676	0	0
15	55	635	41	178.35
20	50	587	89	387.15
25	45	535	141	613.35
30	40	486	190	826.5
35	35	446	230	1000.5
40	30	402	274	1191.9
45	25	355	321	1396.35
50	20	305	371	1613.85
55	15	264	412	1792.2
60	10	215	461	2005.35

almost twice the observed values obtained using 2 m long fiber. This shows that the temperature-dependent pixel variation is computable and proving that the OCT image can be shifted to a focused region by regulating the optical path delay of the traveling laser beam. In addition, these results confirm that using a longer fiber can move more OCT image position with fewer temperature changes while maintaining linear correlations between the temperature change and shifting of the OCT image.

B. QUANTITATIVE ANALYSIS OF AUTOMATIC TEMPERATURE CONTROL SYSTEM-BASED PATH LENGTH COMPENSATION

To demonstrate the minimum attainable degree of the automatic temperature control system, the displacement of OCT image pixel position is measured while changing the temperature by 0.1 °C with 5 m fiber. And this is followed for measuring the increment of temperature by 0.1, 0.2, 0.3, 0.4, and 0.5 °C from the stable temperature condition, the OCT image position is observed to be displaced by 2, 4, 5, 7 and 9 pixels, respectively, which are shown in Fig. 5(a)-(f). The peak intensity pixel at reference temperature is 220 demonstrated in Fig. 5(a). Following the temperature increment, the measured pixels of peak intensity are 218, 216, 215, 213 and 211, respectively. To better show the pixel changes with 0.1 °C increments, we combined Fig. 5(a)-(f) and magnified the peak pixel point which is shown in Fig. 5(g). Hence, from these results, it is conclusive that the automatic temperature control system can be used for maintaining the OCT image position with 0.1 °C temperature accuracy, and within a 2-pixel position accuracy in maintaining the OCT image. In addition, if we use other fiber, which is shorter than 5 m, we can more precisely control the pixel changes at the equivalent experimental condition of measuring Fig. 5.

Furthermore, we measured the SNR, since additional stress to optical fiber caused by thermal expansion generates an unexpected noise. However, the acquired SNR measurements revealed that SNR is not affected by automatic temperature control system. The measured SNR at (20, 20), (40, 20) and (60, 20) are 41.6, 42.1 and 42.1 dB which are much the same at all three temperatures. Hence, the varying temperature does not affect the SNR of the signal. In addition, to minimize the control error between regulated temperature and set temperature, stabilization is an essential process at automatic temperature control system. Therefore, the total consumed time to reach the desired temperature by heating mechanism is measured for 5 °C, 10 °C and 15 °C, and stabilization are 21, 22 and 23 sec respectively. Likewise, the time consumed for stabilization and to reach the desired temperature by cooling mechanism is measured for 5 °C, 10 °C and 15 °C, and the total time is taken for stabilization are 17, 15 and 15 sec, respectively. The averaged stabilizing time is 18 sec; this suggests that the stabilization process can be reliably used and applied for any randomly set temperature for controlling a wide range of path length compensation. Furthermore, whenever the set temperature is changed at a non-stabilized state, the optical fiber temperature is changed immediately and it is stabilized according to the final set value. Hence, the repeatability of the automatic temperature control system is not limited by number of consecutive operations.

C. 2D-OCT IMAGES OF HUMAN RETINA OBTAINED USING AN AUTOMATIC TEMPERATURE CONTROL SYSTEM

To evaluate the applicability of the automatic temperature control system in ophthalmology studies and clinical practice, we imaged three healthy human volunteers (male, 25-30 years) for OCT imaging using the proposed method, and the obtained results are shown in Fig. 6. As the uniqueness of an individual sight and the distance between the lens and retina (vitreous body in the eye) varies from one person to another, this, in turn, makes the (optical path) light travelled by the OCT beam within the eye different from one individual to another [38]. This makes it a necessary step to adjust the

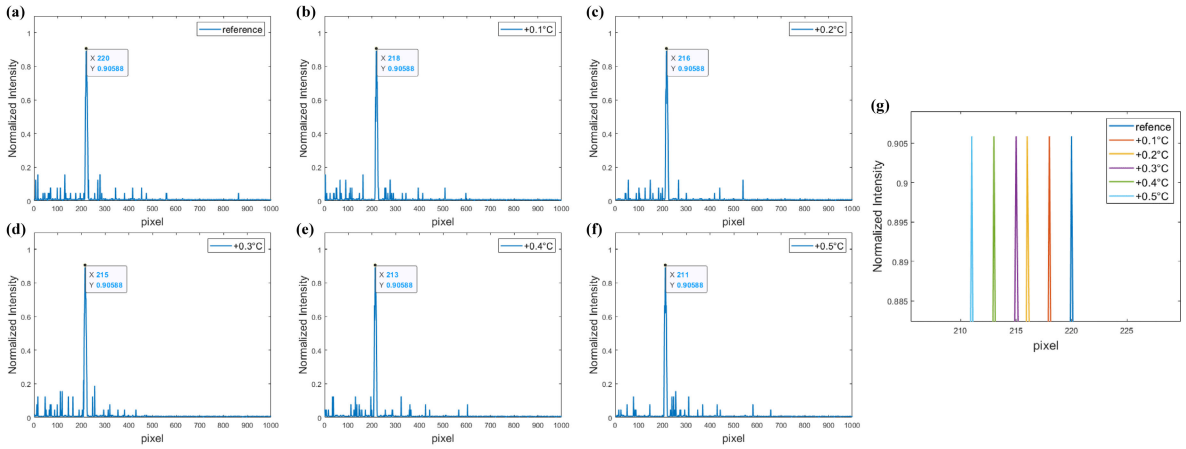

FIGURE 5. Quantitative analysis of pixel changes with 0.1 °C increments from 0.1 °C to 0.5 °C from the reference temperature. (a)-(f) are A-scan graph of mirror images attained at 6 different temperatures that differ by 0.1 °C. (g) demonstrates combined A-scan graph, which magnified the peak pixel changes at aforementioned temperature conditions.

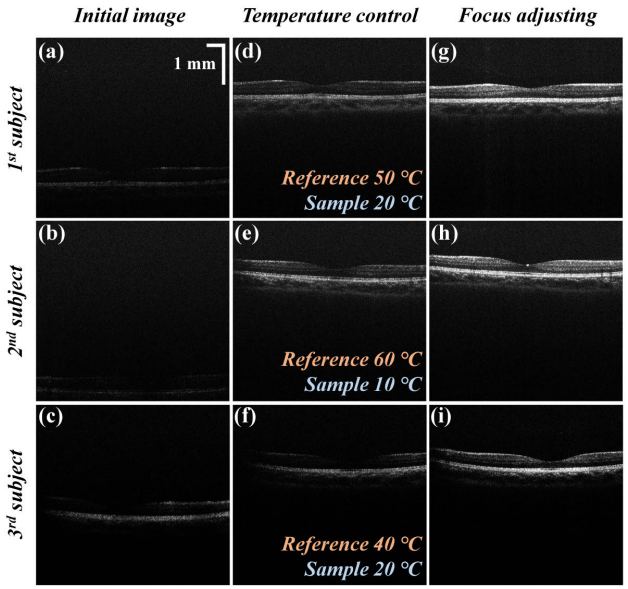

FIGURE 6. Retina OCT images obtained using the automatic temperature control system to change the OCT image position. (a)-(c) are initial images obtained at (20, 20). (d)-(f) are results of temperature control at (50, 20), (60, 10) and (40, 20) respectively. The result of focus adjusting by changing the position of the lens that comprises the beam expander at the sample arm are shown in (g)-(i).

total optical path travelled by the OCT scanning beam in the reference and sample arms in order to obtain a well-focused retinal image. In this study, the compensation of path length difference for the reference and sample arms is attained by the proposed automatic temperature control system.

Fig. 6(a)-(c) are the initial retina images obtained at (20, 20) which show different locations depending on the subject. To adjust the OCT images to an identical focal point, we changed the temperatures of the reference arm and sample arm accordingly to shift the OCT image to its initial position. Fig. 6(d)-(f) are the images acquired at temperatures of (50, 20), (60, 10), and (40, 20), respectively. The specific temperature applied differently for these subjects demonstrates that the positional change of the OCT image through automatic temperature control system can be flexibly adapted as per the situation. After collecting these images, the focus is re-adjusted by changing the position of the beam expander lens in the sample arm. The focus adjusted retina images are shown in Fig. 6(g)-(i). The process of acquiring an OCT image of the human retina through temperature control and focus adjustment is demonstrated in Video. 1. These results demonstrate that the path length control with an automatic temperature control system is possible for any sample, and has demonstrated the possible applicability of the proposed system can be utilized varied application in real-time.

IV. DISCUSSION

Here, we demonstrated the temperature-based automatic path length compensating method to control the position of OCT image and limit the effect of external temperature of optical fiber. The competency of regulating temperature of optical fiber suggests that the proposed method can control the wide range of pixel in OCT without mechanical movement to adjust the image position. In fact, attempts to minimize the effects of temperature on optical fiber have been previously studied. In addition to the results of aforementioned study, various sensors and fibers have been manufactured and used to limit and measure the natural temperature change of fiber. On the other hand, we maximized the thermal expansion effect of the fiber to locate the image at an intended position. Conventionally, manual movement and motor stage-based control methods are widely used to control the path length. However, as an aspect of total price, there are a weakness about using translation stage is 10 times more expensive than comprising an automatic temperature control system, which costs 17.67 $ to compose. In addition, motorized stage-based control method can overcome the limitation of

manual method, but in order to control a wide range of pixel values, the overall size of system becomes large. In contrast, the presented automatic temperature control technique regulates a larger range of path length compensation and is conducive to the design of a compact system without mechanical movement. Moreover, the results showed that the automatic temperature control system is able to achieve OCT image shift for as minimal as single-pixel, was an efficient means to change the beam path length while maintaining OCT image resolution. In addition, even if the initial position of OCT image is much out of focused point, demonstrated method can precisely compensate the path length difference and reposition the image up to several millimeters. Therefore, the presented method of temperature control of optical fiber is an alternative method to complement the limitations of various conventional position control methods in OCT. In addition, for the field of OCT miniaturization, which is actively developed by various groups [39]–[41], automatic temperature control system can offer a wide compensating range of path length maintaining a small size without spatial limitations. Moreover, according to the emerged needs for applying OCT to various outdoor applications, which includes agriculture [42]–[44], external examination and other on-field experiments, this presented temperature based-path length control method can be successfully applied to conduct an aforementioned outdoor fields while offering an equivalent experimental conditions.

V. CONCLUSION

In conclusion, an automatic path length compensation and limiting the redundant temperature effect for OCT imaging is demonstrated by controlling the external temperature of the optical fiber. We control the overall travel path of the optical beam within the optic fiber by changing the external temperature of fiber. To precisely regulate and to maintain the temperature, an automatic temperature control system was developed using Peltier device, thermistor, solid-state relay, cooling fan, and heat sink. In addition, the built LabVIEW based control software, which used PWM and PID feedback control, enabled an efficient and reliable automatic temperature control system for the OCT image position control. 2D-OCT images, A-scan profiling showed the effective changing of the OCT image position by means of temperature regulation. In addition, we obtained *in vivo* human retina image while changing the temperature respectively in accordance with the initial position of each subject to demonstrate the applicability of our system. The results successfully demonstrate the ability to reach and maintain the desired temperature rapidly and accurately. This suggests that the proposed path length control can effectively compensate for minute ambient and local temperature changes in all application environments. The suggested temperature-based position control method can be widely utilized in various optical imaging fields, where the control of beam path length is essential, and which needs to develop the compact system.

ACKNOWLEDMENT

(Daewoon Seong and Sangyeob Han contributed equally to this work.)

REFERENCES

[1] D. Huang, E. A. Swanson, C. P. Lin, J. S. Schuman, W. G. Stinson, W. Chang, M. R. Hee, T. Flotte, K. Gregory, and C. A. Puliafito, "Optical coherence tomography," *Science*, vol. 254, pp. 1178–1181, Nov. 1991.

[2] A. F. Fercher, W. Drexler, C. K. Hitzenberger, and T. Lasser, "Optical coherence tomography—Principles and applications," *Rep. Prog. Phys.*, vol. 66, no. 2, p. 239, 2003.

[3] W. Drexler, U. Morgner, R. K. Ghanta, F. X. Kärtner, J. S. Schuman, and J. G. Fujimoto, "Ultrahigh-resolution ophthalmic optical coherence tomography," *Nature Med.*, vol. 7, p. 502, Apr. 2001.

[4] M. Wojtkowski, V. Srinivasan, J. G. Fujimoto, T. Ko, J. S. Schuman, A. Kowalczyk, and J. S. Duker, "Three-dimensional retinal imaging with high-speed ultrahigh-resolution optical coherence tomography," *Ophthalmology*, vol. 112, no. 10, pp. 1734–1746, Oct. 2005.

[5] S. Han, M. V. Sarunic, J. Wu, M. Humayun, and C. Yang, "Handheld forward-imaging needle endoscope for ophthalmic optical coherence tomography inspection," *J. Biomed. Opt.*, vol. 13, no. 2, 2008, Art. no. 020505.

[6] M. C. Pierce, J. Strasswimmer, B. H. Park, B. Cense, and J. F. de Boer, "Advances in optical coherence tomography imaging for dermatology," *J. Investigative Dermatol.*, vol. 123, no. 3, pp. 458–463, Sep. 2004.

[7] J. Welzel, "Optical coherence tomography in dermatology: A review," *Skin Res. Technol.*, vol. 7, no. 1, pp. 1–9, Feb. 2001.

[8] S. Lee, K. Son, J. Park, J. Lee, S. H. Kang, R. E. Wijesinghe, P. Kim, J. H. Hwang, S. Park, B.-J. Yun, M. Jeon, K.-B. Lee, and J. Kim, "Non-ionized, high-resolution measurement of internal and marginal discrepancies of dental prosthesis using optical coherence tomography," *IEEE Access*, vol. 7, pp. 6209–6218, 2019.

[9] Z. Meng, X. S. Yao, H. Yao, Y. Liang, T. Liu, Y. Li, G. Wang, and S. Lan, "Measurement of the refractive index of human teeth by optical coherence tomography," *J. Biomed. Opt.*, vol. 14, no. 3, 2009, Art. no. 034010.

[10] T.-H. Tsai, J. Fujimoto, and H. Mashimo, "Endoscopic optical coherence tomography for clinical gastroenterology," *Diagnostics*, vol. 4, no. 2, pp. 57–93, 2014.

[11] J. M. Poneros, S. Brand, B. E. Bouma, G. J. Tearney, C. C. Compton, and N. S. Nishioka, "Diagnosis of specialized intestinal metaplasia by optical coherence tomography," *Gastroenterology*, vol. 120, pp. 7–12, Jan. 2001.

[12] M. Taniwaki, M. D. Radu, S. Zaugg, N. Amabile, H. M. Garcia-Garcia, K. Yamaji, E. Jørgensen, H. Kelbæk, T. Pilgrim, C. Caussin, T. Zanchin, A. Veugeois, U. Abildgaard, P. Jüni, S. Cook, K. C. Koskinas, S. Windecker, and L. Räber, "Mechanisms of very late drug-eluting stent thrombosis assessed by optical coherence tomography," *Circulation*, vol. 133, no. 7, pp. 650–660, Feb. 2016.

[13] G. J. Tearney, I.-K. Jang, D.-H. Kang, H. T. Aretz, S. L. Houser, T. J. Brady, K. Schlendorf, M. Shishkov, and B. E. Bouma, "Porcine coronary imaging *in vivo* by optical coherence tomography," *Acta Cardiol.*, vol. 55, no. 4, pp. 233–237, 2000.

[14] P. J. Rosenfeld, A. A. Moshfeghi, and C. A. Puliafito, "Optical coherence tomography findings after an intravitreal injection of bevacizumab (Avastin) for neovascular age-related macular degeneration," *Ophthalmic Surg., Lasers Imag. Retina*, vol. 36, no. 4, pp. 331–335, Jul. 2005.

[15] G. Gregori, R. W. Knighton, C. A. Puliafito, J. E. Legarreta, O. S. Punjabi, and G. A. Lalwani, "Macular thickness measurements in normal eyes using spectral domain optical coherence tomography," *Ophthalmic Surg., Lasers Imag.*, vol. 39, no. 7, pp. S43–S49, Jul. 2008.

[16] T. Horiguchi and M. Tateda, "BOTDA-nondestructive measurement of single-mode optical fiber attenuation characteristics using Brillouin interaction: Theory," *J. Lightw. Technol.*, vol. 7, no. 8, pp. 1170–1176, Aug. 1989.

[17] P. Russell, "Photonic crystal fibers," *Science*, vol. 299, pp. 358–362, Jan. 2003.

[18] J. C. Knight, T. A. Birks, P. S. J. Russell, and D. M. Atkin, "All-silica single-mode optical fiber with photonic crystal cladding," *Opt. Lett.*, vol. 21, no. 19, pp. 1547–1549, Oct. 1996.

[19] J. Broeng, D. Mogilevstev, S. E. Barkou, and A. Bjarklev, "Photonic crystal fibers: A new class of optical waveguides," *Opt. Fiber Technol.*, vol. 5, no. 3, pp. 305–330, Jul. 1999.

[20] P. Kaiser and H. W. Astle, "Low-loss single-material fibers made from pure fused silica," *Bell Syst. Tech. J.*, vol. 53, no. 6, pp. 1021–1039, Jul. 1974.
[21] D. Gloge and E. A. J. Marcatili, "Multimode theory of graded-core fibers," *Bell Syst. Tech. J.*, vol. 52, no. 9, pp. 1563–1578, Nov. 1973.
[22] Y. Choi, C. Yoon, M. Kim, T. D. Yang, C. Fang-Yen, R. R. Dasari, K. J. Lee, and W. Choi, "Scanner-free and wide-field endoscopic imaging by using a single multimode optical fiber," *Phys. Rev. Lett.*, vol. 109, no. 20, Nov. 2012, Art. no. 203901.
[23] K. Suzuki, H. Kubota, S. Kawanishi, M. Tanaka, and M. Fujita, "Optical properties of a low-loss polarization-maintaining photonic crystal fiber," *Opt. Express*, vol. 9, no. 13, pp. 676–680, Dec. 2001.
[24] L. G. Cohen and J. W. Fleming, "Effect of temperature on transmission in lightguides," *Bell Syst. Tech. J.*, vol. 58, no. 4, pp. 945–951, Apr. 1979.
[25] N. Lagakos, J. A. Bucaro, and J. Jarzynski, "Temperature-induced optical phase shifts in fibers," *Appl. Opt.*, vol. 20, no. 13, pp. 2305–2308, Jul. 1981.
[26] G. B. Hocker, "Fiber-optic sensing of pressure and temperature," *Appl. Opt.*, vol. 18, no. 9, pp. 1445–1448, May 1979.
[27] C.-L. Zhao, X. Yang, C. Lu, W. Jin, and M. S. Demokan, "Temperature-insensitive interferometer using a highly birefringent photonic crystal fiber loop mirror," *IEEE Photon. Technol. Lett.*, vol. 16, no. 11, pp. 2535–2537, Nov. 2004.
[28] J. Teng, P. Dumon, W. Bogaerts, H. Zhang, X. Jian, X. Han, M. Zhao, G. Morthier, and R. Baets, "Athermal Silicon-on-insulator ring resonators by overlaying a polymer cladding on narrowed waveguides," *Opt. Express*, vol. 17, no. 17, pp. 14627–14633, Aug. 2009.
[29] R. Leitgeb, C. K. Hitzenberger, and A. F. Fercher, "Performance of Fourier domain vs. time domain optical coherence tomography," *Opt. Express*, vol. 11, no. 8, pp. 889–894, Apr. 2003.
[30] J. F. de Boer, B. Cense, B. H. Park, M. C. Pierce, G. J. Tearney, and B. E. Bouma, "Improved signal-to-noise ratio in spectral-domain compared with time-domain optical coherence tomography," *Opt. Lett.*, vol. 28, no. 21, pp. 2067–2069, Nov. 2003.
[31] C. E. Saxer, J. F. de Boer, B. H. Park, Y. Zhao, Z. Chen, and J. S. Nelson, "High-speed fiber–based polarization-sensitive optical coherence tomography of *in vivo* human skin," *Opt. Lett.*, vol. 25, no. 18, pp. 1355–1357, 2000.
[32] B. Baumann, E. Götzinger, M. Pircher, H. Sattmann, C. Schütze, F. Schlanitz, C. Ahlers, U. Schmidt-Erfurth, and C. K. Hitzenberger, "Segmentation and quantification of retinal lesions in age-related macular degeneration using polarization-sensitive optical coherence tomography," *J. Biomed. Opt.*, vol. 15, no. 6, 2010, Art. no. 061704.
[33] Y. Huang, X. Liu, C. Song, and J. U. Kang, "Motion-compensated handheld common-path Fourier-domain optical coherence tomography probe for image-guided intervention," *Biomed. Opt. Express*, vol. 3, no. 12, pp. 3105–3118, Dec. 2012.
[34] C. Song, P. L. Gehlbach, and J. U. Kang, "Active tremor cancellation by a 'smart' handheld vitreoretinal microsurgical tool using swept source optical coherence tomography," *Opt. Express*, vol. 20, no. 21, pp. 23414–23421, 2012.
[35] J. Khurgin, "Adiabatically tunable optical delay lines and their performance limitations," *Opt. Lett.*, vol. 30, no. 20, pp. 2778–2780, 2005.
[36] J. B. Khurgin, "Dispersion and loss limitations on the performance of optical delay lines based on coupled resonant structures," *Opt. Lett.*, vol. 32, no. 2, pp. 133–135, Jan. 2007.
[37] N. Ravichandran, R. Wijesinghe, S.-Y. Lee, K. Choi, M. Jeon, H.-Y. Jung, and J. Kim, "Non-destructive analysis of the internal anatomical structures of mosquito specimens using optical coherence tomography," *Sensors*, vol. 17, no. 8, p. 1897, 2017.
[38] M. Pircher, E. Götzinger, and C. K. Hitzenberger, "Dynamic focus in optical coherence tomography for retinal imaging," *J. Biomed. Opt.*, vol. 11, no. 5, 2006, Art. no. 054013.
[39] P. Pande, R. L. Shelton, G. L. Monroy, R. M. Nolan, and S. A. Boppart, "Low-cost hand-held probe for depth-resolved low-coherence interferometry," *Biomed. Opt. Express*, vol. 8, no. 1, pp. 338–348, Jan. 2017.
[40] R. E. Wijesinghe, S.-Y. Lee, N. K. Ravichandran, S. Han, H. Jeong, Y. Han, H.-Y. Jung, P. Kim, M. Jeon, and J. Kim, "Optical coherence tomography-integrated, wearable (backpack-type), compact diagnostic imaging modality for *in situ* leaf quality assessment," *Appl. Opt.*, vol. 56, no. 9, pp. D108–D114, Mar. 2017.
[41] G. L. Monroy and J. Won, "Clinical translation of handheld optical coherence tomography: Practical considerations and recent advancements," *J. Biomed. Opt.*, vol. 22, no. 12, Dec. 2017, Art. no. 121715.
[42] Y. Zhou, J. Mao, T. Liu, W. Zhou, and Z. Chen, "Discriminating hidden bruises in loquat by attenuation coefficients estimated from optical coherence tomography images," *Postharvest Biol. Technol.*, vol. 130, pp. 1–6, Aug. 2017.
[43] R. E. Wijesinghe, S.-Y. Lee, P. Kim, H.-Y. Jung, M. Jeon, and J. Kim, "Optical sensing method to analyze germination rate of capsicum annum seeds treated with growth-promoting chemical compounds using optical coherence tomography," *J. Biomed. Opt.*, vol. 22, no. 9, Jan. 2017, Art. no. 091502.
[44] A. Rateria, M. Mohan, K. Mukhopadhyay, and R. Poddar, "Investigation of Puccinia triticina contagion on wheat leaves using swept source optical coherence tomography," *Optik*, vol. 178, pp. 932–937, Feb. 2019.

DAEWOON SEONG received the B.E. degree from the School of Electronics Engineering, Kyungpook National University, Daegu, South Korea. He is currently a MD Researcher with the School of Electronics Engineering, Kyungpook National University. His research focuses on developing optical imaging techniques, photoacoustic microscopy, and optical coherence tomography for medical application.

SANGYEOB HAN received the Ph.D. degree from the School of Electronics Engineering, Kyungpook National University, Daegu, South Korea. His research background includes optical imaging techniques, photoacoustic microscopy, optical coherence tomography, and multiphoton microscopy.

DEOKMIN JEON received the B.E. degree in electronics engineering from Kyungil University, Daegu, South Korea, and the M.Sc. and Ph.D. degrees in electronics engineering from Kyungpook National University, Daegu. His research interest is in the development of the novel biomedical and industrial imaging technique using advanced optical materials, including optical coherence tomography, vision inspection, photoacoustic imaging, and other optical applications.

YOONSEOK KIM received the B.E. degree in electronics engineering from Kyungpook National University, Daegu, South Korea, in 2018. He is currently a MD Researcher with the Electronics Engineering Department, Kyungpook National University. His research interests are in development of optical system for medical application and image processing and development and applications for spectral domain optical coherence tomography.

RUCHIRE ERANGA WIJESINGHE received the B.Sc. and Ph.D. degrees in electronics engineering from Kyungpook National University, Daegu, South Korea, in 2012 and 2018, respectively. He is currently an Assistant Professor with the Department of Biomedical Engineering, Kyungil University. His research interests are in the development of high-resolution novel biological and biomedical imaging techniques, including optical coherence tomography and microscopy for clinical utility.

NARESH KUMAR RAVICHANDRAN received the Bachelor of Engineering degree in electronics and communication engineering from St. Peter's University, Tamil Nadu, India, and the M.Sc. and Ph.D. degrees in electronics engineering from Kyungpook National University, Daegu, South Korea. He is currently working as a Postdoctoral Researcher with the Department of Center for Scientific Instrumentation, Korea Basic Science Institute (KBSI). His research interest is in the developing and optimizing novel bio-imaging techniques with possible applications in medical and biomedical investigations, agronomic studies, entomological studies, industrial applications, and for dental research and clinical trials. His area of expertise lies in but not limited to, building and implementations of optical coherence tomography systems and non-linear microscopy for medical and biomedical research.

JAEYUL LEE is currently pursuing the Ph.D. degree with the School of Electronics Engineering, Kyungpook National University, Daegu, South Korea. His research interests are in the development of high-resolution novel imaging techniques and optical imaging techniques, including photoacoustic microscopy, optical coherence tomography, handheld instruments, and their biomedical applications.

JUNSOO LEE received the B.E. degree in electronics engineering from Kyungpook National University, Daegu, South Korea, in 2018. He is currently a MD Researcher with the Electronics Engineering Department, Kyungpook National University. His research interests are in development of optical system for medical application, photoacoustic tomography, and development and applications for spectral domain optical coherence tomography.

PILUN KIM received the Ph.D. degree from the Department of Medical and Biological Engineering, Kyoungpook National University, in 2011. He is currently a Researching Visiting Professor with the Institute of Biomedical Engineering, Kyungpook National University. He is interested in translating new technologies from the research field to the application field, such as clinic and industrial and making its productization. His main interests are biomedical device development, optical coherence tomography, and digital image processing.

DONG-EUN LEE worked as an Assistant Professor at the School of Engineering, Southern Illinois University Edwardsville (SIUE), USA. He is currently a Full Professor with tenure in both the School of Architecture and Civil Engineering and the Robot and Smart System Engineering at Kyungpook National University, South Korea. He is also the Chief of the Intelligent Costruction Automation Center nominated by the Ministry of Science and ICT. His specialty includes automation in construction, construction robot, optimization, stochastic simulation and quantitative analysis, and so on.

MANSIK JEON (Member, IEEE) received the Ph.D. degree in electronics engineering from Kyungpook National University, Daegu, South Korea, in 2011. He is currently an Assistant Professor with the School of Electronics Engineering, Kyungpook National University. His research interests are in the development of nonionizing and noninvasive novel biomedical imaging techniques, including photoacoustic tomography, photoacoustic microscopy, optical coherence tomography, ultrasonic imaging, handheld scanner, and their clinical applications.

JEEHYUN KIM (Member, IEEE) received the Ph.D. degree in biomedical engineering from The University of Texas at Austin, USA, in 2004. He has worked as a Postdoctoral Researcher at the Beckman Laser Institute, University of California at Irvine, Irvine. He is currently an Associate Professor with Kyungpook National University, Daegu, South Korea. His research interest is in biomedical imaging and sensing, neuroscience studies using multiphoton microscopy, photo-acoustic imaging, and other novel applications of sensors.